AIAA JOURNAL
Vol. 40, No. 2, February 2002

Vortex Structure on a Delta Wing at High Angle of Attack

M. Özgören*
Lehigh University, Bethlehem, Pennsylvania 18015
B. Sahin†
Cukurova University, Balcali 01330 Adana, Turkey
and
D. Rockwell‡
Lehigh University, Bethlehem, Pennsylvania 18015

The structure of the leading-edge vortex from a delta wing at high angle of attack is addressed using a scanning laser version of high-image-density particle image velocimetry. Emphasis is on the global patterns of instantaneous vorticity. These patterns are related to distributions of averaged and fluctuating velocity and vorticity. At low angle of attack, in the absence of vortex breakdown, it is possible to detect a total of five distinct layers of vorticity; they all exhibit small-scale concentrations of azimuthal vorticity. Immediately downstream of the trailing edge of the wing, larger-scale vorticity concentrations appear in the outermost vorticity layers. At sufficiently high angle of attack, vortex breakdown evolves from the innermost two vorticity layers. For all of these classes of vortical structures, the values of dimensionless wavelength and circulation are assessed. Moreover, the onset of vortex breakdown is interpreted in terms of both instantaneous and averaged patterns of velocity and vorticity. These considerations lead to a direct comparison of vorticity-based and stagnation criteria for breakdown. In turn, these criteria are linked to the onset of regions of fluctuating vorticity in the initial region of breakdown.

Nomenclature

C = chord of delta wing
D_{PR} = diameter of vortex measured at interface of vorticity layers P and R at a location before the onset of breakdown (i.e., a distance $0.375C$ upstream of trailing edge of wing)
D_v = characteristic diameter of vortex before onset of breakdown at location a distance of $0.6C$ upstream of trailing edge of wing
D_v^* = characteristic diameter of vortex before onset of breakdown at location a distance of $0.375C$ upstream of trailing edge of wing and characteristic diameter of vortex at trailing edge
M = magnification
Re = Reynolds number, $Re = U_\infty C/\nu$
U_{ref} = reference velocity
U_∞ = freestream velocity
V = total instantaneous velocity
$\langle V \rangle$ = averaged velocity
w = axial velocity of vortex
z = axial coordinate along centerline of vortex
α = angle of attack of delta wing
Γ^* = dimensionless circulation, $\Gamma^* = \Gamma/\pi U_{ref} D_v$
Λ = sweep angle of delta wing
λ = wavelength
ν = kinematic viscosity
σ = radial coordinate from centerline of vortex
ω = vorticity
$\langle \omega \rangle$ = averaged vorticity
ω_{rms} = root mean square of vorticity fluctuation

Received 29 February 2000; revision received 13 June 2000; accepted for publication 15 June 2001.

*Visiting Research Scientist, Department of Mechanical Engineering and Mechanics, 354 Packard Laboratory, 19 Memorial Drive West; on leave from Department of Mechanical Engineering, Cukurova University, Balcali 01330 Adana, Turkey.
†Professor, Department of Mechanical Engineering.
‡Paul B. Reinhold Professor, Department of Mechanical Engineering and Mechanics, 354 Packard Laboratory, 19 Memorial Drive West. Member AIAA.

Introduction

Buffeting of Aerodynamic Surfaces Due to Unsteadiness of Vortices

THE unsteady structure of the vortex from a swept leading edge has important consequences for the time-dependent loading. (i.e., buffeting) of both the wing and the tail of an aircraft. Such loading is due to the convection of patterns of vorticity past the wing or tail. The best-known vorticity pattern arises from vortex breakdown; it often takes the form of a helical spiral. The relationship between the qualitative pattern(s) of vorticity due to vortex breakdown and the surface buffeting has been addressed by Gursul and Xie[1]; this work was preceded by a wide variety of investigations, originating with the works of Earnshaw and Lawford[2] and Mabey.[3] In addition to vortex breakdown, other origins of steady and unsteady vorticity concentrations can occur on a leading-edge vortex, as assessed by Riley and Lowson.[4] Furthermore, a rotating vortex in the absence of a leading edge can give rise to patterns of three-dimensional vorticity, as described by Sreedhar and Ragab.[5] Irrespective of the physical origin of a vorticity pattern, it can potentially contribute to the buffeting of an adjacent aerodynamic surface as long as it exhibits unsteadiness. In the sections that follow, the possible origins of vorticity patterns are described in further detail to provide a basis for defining the unresolved issues and the objectives of the present investigations.

Vortex Breakdown on a Delta Wing

The theoretical framework, as well as experimental investigations of vortex breakdown are addressed in the reviews and investigations of Sarpkaya,[6–8] Hall,[9] Liebovich,[10,11] Escudier,[12] Brown and Lopez,[13] Lopez and Perry,[14] Delery,[15] Visbal,[16] and Rusak et al.[17] An interesting observation, as demonstrated by qualitative flow visualization, is the existence of the same general form of instability of the breakdown region over a very wide range of Reynolds number. For example, the dye visualization of vortex breakdown on a delta wing at low Reynolds number $Re = 0.65 \times 10^4$ by Wérle[18] exhibits the same general form as smoke visualization at $Re = 5.8 \times 10^5$ by Pagan and Solignac.[19] That is, the occurrence of a spirallike instability,

apparently arising from a predominantly inviscid instability mechanism, is clearly evident in both cases. This observation suggests that numerical and experimental investigations at varying values of Reynolds number should reveal certain common mechanisms of unsteadiness in the breakdown region.

In recent years, global experimental approaches to characterizing vortex breakdown on a delta wing have involved the investigations of Towfighi and Rockwell[20] and Lin and Rockwell.[21] These investigations characterized instantaneous patterns of vorticity and streamline topology associated with breakdown. They were guided by the theoretical work of Brown and Lopez,[13] who formulated a relationship between alteration of the vorticity field in the vicinity of vortex breakdown and occurrence of a stagnation condition along the axis of the vortex. As addressed in Towfighi and Rockwell,[20] the appropriate equation of Brown and Lopez[13] is

$$w(o, z) = \frac{1}{2}\int_{-\infty}^{\infty}\int_{0}^{\infty} \frac{\sigma^2\omega(\sigma, z')}{[\sigma^2 + (z - z')^2]^{\frac{3}{2}}}\,\mathrm{d}\sigma\,\mathrm{d}z' \qquad (1)$$

In this equation, the axial velocity along the centerline of the vortex is designated as $w(o, z)$, the coordinate z is along the axis of the vortex, the radial coordinate σ is measured from the centerline of the vortex, and ω is the azimuthal vorticity at location (σ, z). The important feature of this equation is, according to Brown and Lopez,[13] that only when the azimuthal vorticity becomes negative can a zero or negative velocity occur on the axis of the vortex. This concept is suggested in the experiments Towfighi and Rockwell[20] and in the numerical simulation of Visbal.[22] However, the nature of rapid distortion of the velocity field and the alteration of patterns of azimuthal vorticity in both instantaneous and averaged forms, as well as root-mean-square vorticity fluctuations in the region of vortex breakdown, have not been established.

Instabilities in the Vortex from a Delta Wing

Although vortex breakdown is generally attributed to be the primary source of generation of vorticity concentrations, two alternate and apparently unrelated mechanisms occur on the outer periphery of the vortex, leading to generation of streamwise vorticity concentrations in the shear layer formed from the leading edge. Riley and Lowson[4] provide an assessment of these instabilities.

The first type is a time-varying instability, which is analogous to the classical Kelvin–Helmholtz instability of the corresponding two-dimensional separated shear layer. This instability, which gives rise to apparent concentrations of vorticity in the separating shear layer from the windward side of the wing, has been characterized using qualitative visualization by Gad-el-Hak and Blackwelder[23,24] and Lowson.[25] The generation of small-scale structures due to separation of the vorticity layer from the leeward side of the wing is demonstrated in the numerical simulations of Gordnier and Visbal[26] and Visbal and Gordnier.[27] In the event that a delta wing is subjected to unsteady rolling motion, vorticity concentrations formed in the shear layers emanating from both the leeward and windward sides of the wing are evident, giving rise to coexisting patterns of counter-rotating vortices, as shown by Cipolla and Rockwell.[28]

The second type of shear-layer instability has a steady form. It can give rise to identifiable, small-scale vortices about the primary vortex formed from the leading edge, as addressed by Payne,[29] Payne et al.,[30] Lowson,[25] and Reynolds and Abtahi.[31] These small-scale vortices apparently take the form of steady longitudinal structures. Laser Doppler anemometry measurements in the crossflow plane on a delta wing by Riley and Lowson[4] define quantitatively the series of vorticity concentrations about the primary vortex due to these longitudinal structures.

Issues and Objectives

To date, the instantaneous, quantitative structure of these classes of vorticity concentrations has not been addressed in relation to those due to vortex breakdown. To be sure, the first type of vorticity concentrations can occur even when the second type is not present; this is expected to be the case at low angle of attack of the wing, when vortex breakdown does not occur. At high angle of attack, not only does vortex breakdown occur within the interior of the vortex, but also three-dimensional flow separation and perhaps associated vorticity concentrations arise from the leeward side of the wing in the vicinity of the trailing edge.[32] The end result of all of these possible origins of vorticity concentrations would be a complex pattern of concentrations that mutually influence each other.

The objective of the present investigation is to identify, then to evaluate quantitatively, coexisting concentrations of azimuthal vorticity, which can arise from several possible origins. Determination of the dimensionless wavelengths and values of circulation of each of these classes of vorticity concentration yields information directly related to the buffet loading of an adjacent aerodynamic surface. It is particularly insightful to employ a technique that provides global, instantaneous patterns of vorticity. A method of high-image-density particle image velocimetry yields these types of representations. In turn, the instantaneous patterns of vorticity can be related to averaged patterns of both vorticity and velocity to provide insight into criteria that dictate the onset of unsteadiness.

Experimental System and Techniques

A delta wing is located in a water channel having a water height of 559 mm. It was mounted at middepth at its midchord on a vertical, streamlined sting, with a width of 3 mm and a length of 38 mm. The fact that the sting did not influence the physics of the phenomena addressed here was verified by extensive dye injection at various locations on the leeward surface of the wing and comparison of the onset of vortex breakdown with established values. The cross-sectional dimensions of the channel were 610×927 mm. Figure 1 provides plan and side views of the delta wing, with $\Lambda = 75$ deg, a thickness of 3.2 mm, and $C = 222$ mm. The bevel angle of the wing was 34 deg; it was beveled only on the windward side. Over the course of the experiment, values of $\alpha = 24$, 30, 32, and 35 deg were employed. For all cases, the value of freestream velocity was maintained constant at 48 mm/s, corresponding to a Reynolds number based on C of $Re = 1.07 \times 10^4$.

A laser-scanning technique of high-image-density particle image velocimetry (PIV)[33] allowed characterization of instantaneous patterns of flow quantities over a plane passing through the centerline of the vortex. The orientation and extent of the scanning laser beam (20 W) that defines the laser sheet of observation is given in Fig. 1. This beam was generated first by transmitting it through a series of steering and focusing optics. The beam then impinged upon a rotating polygonal mirror with eight facets. The effective scanning frequency of the laser beam was 125 Hz. To implement the technique of high-image-density PIV, it is necessary to seed the flow with small particles. In this experiment, hollow plastic spheres, which were metallic coated and had a diameter of 14 μm, were employed as scattering particles. They were essentially neutrally buoyant; moreover,

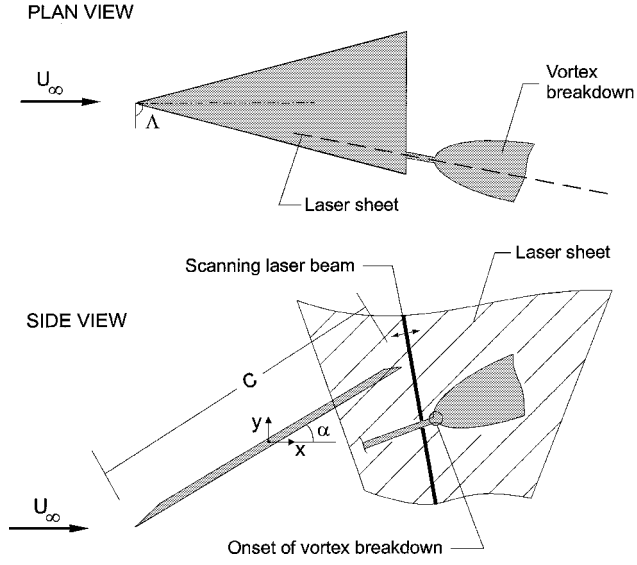

Fig. 1 Schematic of experimental system showing delta wing at high angle of attack and onset of vortex breakdown.

calculations showed that the particle slip was insignificant in the regions of small streamline curvature at the center of the vortex.

A Canon EOS-1 35 mm camera was employed for capturing the multiply exposed particle images generated by successive scans of the laser beam. The shutter speed of the camera was $\frac{1}{25}$ s, and the aperture was $f5$. To capture the critical field of view, the camera lens had a value of $M = 1{:}4.3$. An oscillating bias mirror was deployed immediately in front of the camera lens to avoid issues associated with directional ambiguity. The framing rate of the motor-driven camera was 5.55 frames/s.

Patterns of particle images were recorded on high-resolution 35 mm film (300 lines/mm). These negatives were digitized with a resolution of 125 pixels/mm. The velocity field was obtained by applying a single-frame crosscorrelation technique to the patterns of particle images. The size of the interrogation window was 90×90 pixels, with 50% overlap. The criterion of high image density was well exceeded by ensuring that about 40–60 particle images were located within the interrogation window. The total number of velocity vectors was 5734 per frame. During postprocessing, a Gaussian filter with a factor of $p = 1.3$ was applied to the velocity field. No additional filtering of the data was carried out. The effective grid size in the physical plane of the laser sheet was 1.53×1.53 mm. The field of view in the images shown here varies from 62×144 mm to 104×144 mm, depending on the region of interest. The estimated uncertainty of velocity and vorticity is less than 1 and 6%, respectively.

With sequences of PIV images at hand, it is possible to evaluate averages of V and ω. The following definitions were employed for these averages:

$$\langle V \rangle = \frac{1}{N} \sum_{n=1}^{N} V_n(x, y) \tag{2a}$$

$$\langle \omega \rangle = \frac{1}{N} \sum_{n=1}^{N} \omega_n(x, y) \tag{2b}$$

$$\langle \omega_{\text{rms}} \rangle = \left\{ \frac{1}{N} \sum_{n=1}^{N} [\omega_n(x, y) - \langle \omega(x, y) \rangle]^2 \right\}^{\frac{1}{2}} \tag{2c}$$

in which N is the total number of PIV images. Averaged representations were constructed from averaging a total of 36 images.

In this investigation, values of dimensionless circulation and wavelength are calculated. The velocity and length scales used for normalization are as follows: U_{ref} corresponds to the velocity in the undisturbed region of the freestream, at a horizontal distance of $3.6C$ and a vertical distance of $4.1C$ from the midchord of the wing. The reference diameter D_v of the leading-edge vortex is defined as the distance between maximum-positive and maximum-negative values of vorticity across the leading-edge vortex; it is evaluated at a distance $0.6C$ upstream of the trailing edge of the wing at $\alpha = 24$ deg. Further definitions of characteristic vortex diameter, based on the same concept as for D_v, are defined in subsequent sections of the text. The maximum values of uncertainty of the dimensionless wavelength λ/D_v and circulation $\Gamma^* = \Gamma/\pi\ U_{\text{ref}}\ D_v$ are estimated to be 4 and 7%, respectively.

Structure of Leading-Edge Vortex

Overview of Instantaneous and Averaged Patterns of Vorticity and Velocity

The structure of the leading-edge vortex upstream of the trailing edge of the wing is shown in Fig. 2. Patterns of ω, $\langle \omega \rangle$, ω_{rms}, and $\langle V \rangle$ are directly compared. Referring first to the pattern of $\langle \omega \rangle$, a total of five distinct layers are detectable. They are designated as P^+, P^-, R^+, R^-, and S^+, respectively. Layers P^+, R^+, and S^+ are all positive (thick white lines), whereas layers P^- and R^- are negative (thin white lines). Layers P^- and P^+ correspond to the innermost portion of the vortex and, at sufficiently high angle of attack, appear to be associated with vortex breakdown. Layers R^+ and R^- bound the innermost layers P^- and P^+. Finally, layer S^+ is immediately adjacent to the surface of the wing. The patterns of ω corresponding to these averaged layers are shown in the top image of Fig. 2. Detectable, small-scale concentrations of azimuthal vorticity are discernible. Referring to the image of averaged fluctuating vorticity, represented by ω_{rms}, it is evident that relatively high vorticity fluctuations occur in the region defined by averaged vorticity layers P^- and R^+, and discernible fluctuations are evident at the junction of layers P^+ and R^-, as well as at the wall layer S^+. The pattern of $\langle V \rangle$ indicates a continuous decrease of velocity along the centerline of the vortex, but does not show existence of a wake like region, which would be characteristic of vortex breakdown.

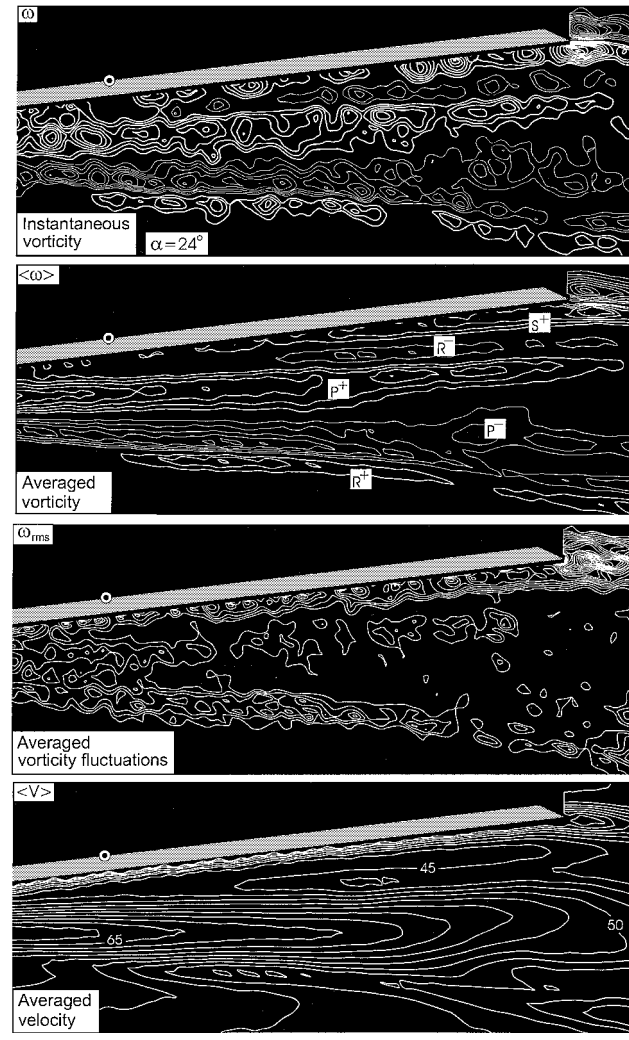

Fig. 2 Patterns of instantaneous ω, $\langle \omega \rangle$, and ω_{rms}, in comparison with $\langle V \rangle$ at $\alpha = 24$ deg. Minimum and incremental values of instantaneous ω are 1 and 0.75 s^{-1}, of $\langle \omega \rangle$ are 1 and 0.75 s^{-1}, and of ω_{rms} are 0.75 and 0.1 s^{-1}. For contours of $\langle V \rangle$, units of numerical values designated on contour lines are mm/s and incremental value between contours is 2.5 mm/s.

The patterns shown in Fig. 2 evolve to the forms exhibited in Fig. 3a at locations downstream of the trailing edge of the wing. Most notably, the averaged layers P^- and R^+ eventually exhibit distinct concentrations of vorticity, designated as A^+, A^- through D^+, D^-. It should be emphasized that these concentrations occur in the absence of vortex breakdown. That is, the pattern of ω does not indicate the onset of pronounced, alternating patterns of vorticity within the central region of the vortex. The pattern of ω_{rms} shows relatively high levels of fluctuating vorticity corresponding to the generation of the vorticity concentrations A through D, as designated in the pattern of ω.

The consequences of increase in angle of attack are exhibited in Fig. 3b. In this case, $\alpha = 30$ deg. The pattern of instantaneous vorticity shows even more pronounced concentrations in the outer region of the vortex, again designated as A^+, A^- through D^+. At this higher angle of attack, pronounced vortex breakdown is clearly

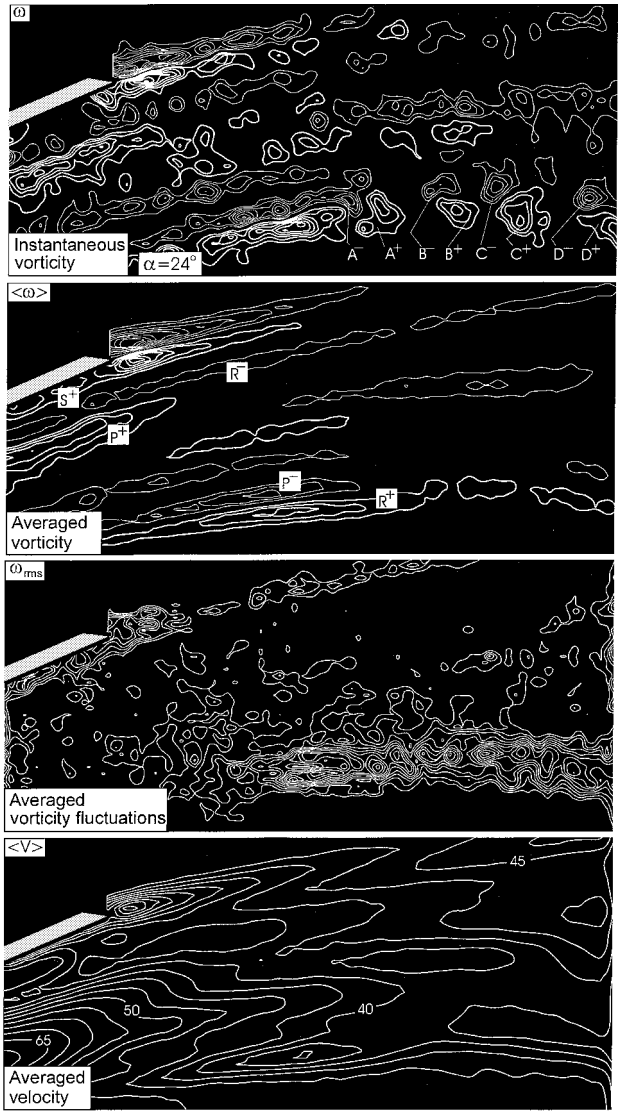

Fig. 3a Patterns of instantaneous ω, $\langle\omega\rangle$, and ω_{rms}, in comparison with $\langle V\rangle$ at $\alpha = 24$ deg. Minimum and incremental values of instantaneous ω are 1 and 0.75 s^{-1}, of $\langle\omega\rangle$ are 1 and 0.75 s^{-1}, and of ω_{rms} are 0.75 and 0.125 s^{-1}. For contours of $\langle V\rangle$, units of numerical values designated on contour lines are mm/s and incremental value between contours is 2.5 mm/s.

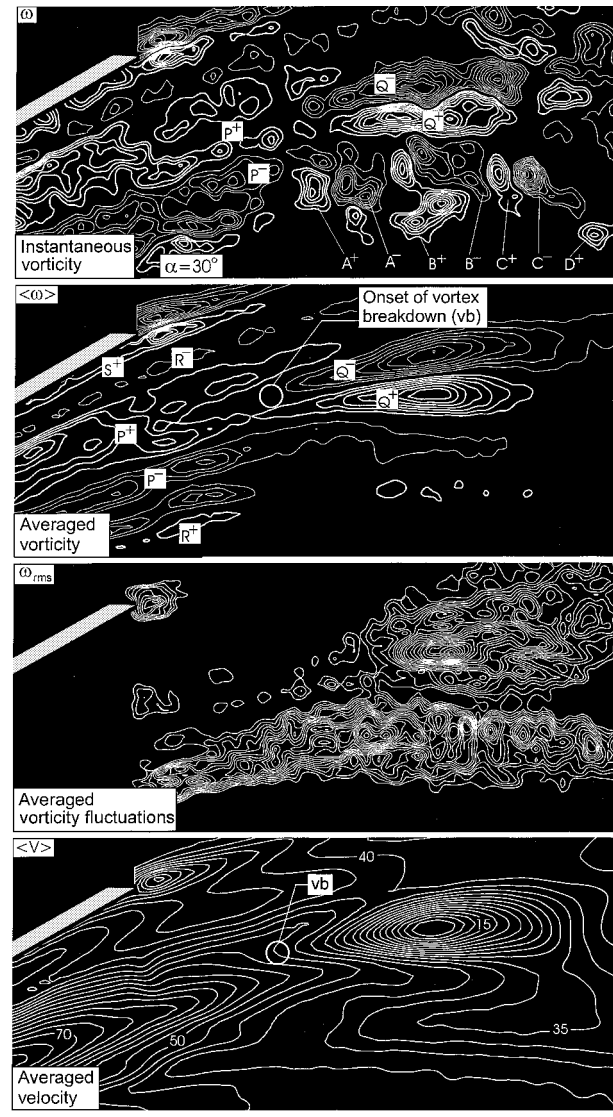

Fig. 3b Patterns of instantaneous ω, $\langle\omega\rangle$, and ω_{rms}, in comparison with $\langle V\rangle$ at $\alpha = 30$ deg. Minimum and incremental values of instantaneous ω are 1 and 0.75 s^{-1}, of $\langle\omega\rangle$ are 1 and 0.75 s^{-1}, and of ω_{rms} are 0.75 and 0.125 s^{-1}. For contours of $\langle V\rangle$, units of numerical values designated on contour lines are mm/s and incremental value between contours is 2.5 mm/s.

evident. The vortical structures arising from the onset of vortex breakdown are designated as Q^+ and Q^-. They appear to evolve from the centermost vorticity layers P^+ and P^-. Note that the switch in sign of azimuthal vorticity at the onset of vortex breakdown is in accord with that defined previously by Towfighi and Rockwell[20] and is compatible with the theoretical prediction of Brown and Lopez.[13] The pattern of $\langle\omega\rangle$ clearly shows the switch in azimuthal vorticity as the onset of vortex breakdown occurs from layers P^+ and P^-. Examination of ω_{rms} shows relatively high levels, in both the region corresponding to vortex breakdown and the region associated with the onset and development of the counter-rotating vortex pairs.

The corresponding patterns at a still higher value of $\alpha = 32$ deg are exhibited in Fig. 3c. The vorticity concentrations A^+ through C^- are indeed pronounced and, in this case, occur near the onset of vortex breakdown, as for Fig. 3b. In Fig. 3c, where α is only 2 deg larger than for Fig. 3b, the onset of breakdown has moved upstream of the trailing edge of the wing. The pattern of $\langle\omega\rangle$ shows that the switch in sign of the azimuthal vorticity occurs sharply at a well-defined location, in contrast to the more gradual transformation at the lower angle of attack in Fig. 3b. The pattern of ω_{rms} exhibits relatively high vorticity levels at the onset of vortex breakdown and at the edges of the breakdown bubble. In addition, a layer of relatively high fluctuating vorticity occurs in the region between the breakdown bubble and the freestream; it is, of course, associated with the array of vorticity concentrations in the outer layer of the vortex. Finally, all of these phenomena associated with the patterns of vorticity involve an abrupt transformation of the field $\langle V\rangle$ from a jetlike flow to a wakelike flow involving a region of negative velocity immediately after the onset of vortex breakdown.

Wavelengths and Circulation of Characteristic Vorticity Concentrations

Figure 3d directly compares representative images of instantaneous vorticity from the lowest to the highest angle of attack. Of particular interest for buffeting of aerodynamic surfaces are the streamwise λ between adjacent vortical structures of like sign, and the Γ^* of these vortical structures. In all images shown in Fig. 3d, it is evident that small-scale, lower-level concentrations of vorticity are typically detectable in the vorticity layers upstream of vortex breakdown. In preceding figures, these layers of vorticity were designated as P^+, P^-, R^+, R^- and S^+. At each angle of attack, a total of three consecutive images of instantaneous vorticity were considered, and the averaged value of λ between adjacent concentrations was evaluated. These values of λ are normalized by D_v, evaluated as

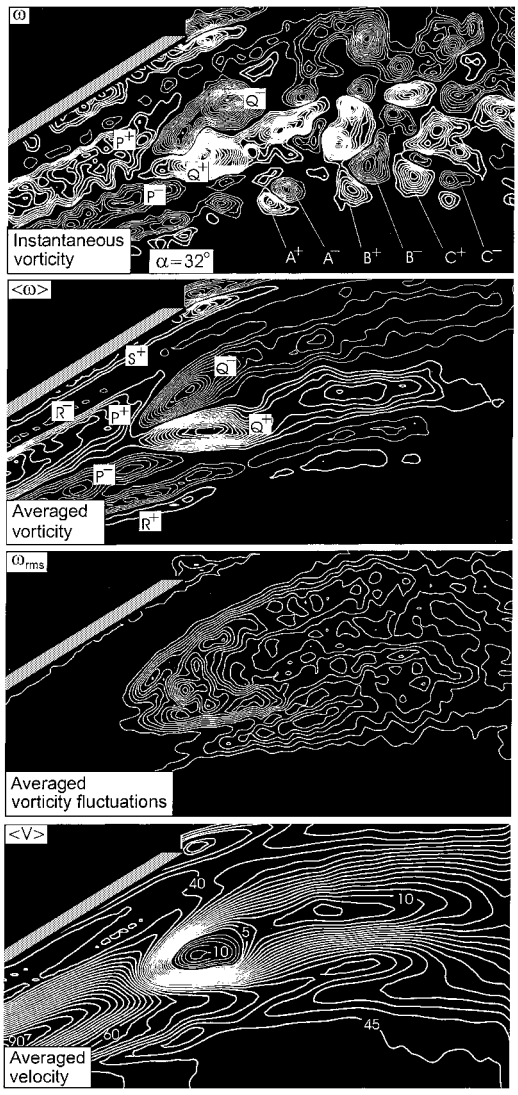

Fig. 3c Patterns of instantaneous ω, $\langle\omega\rangle$, and $\omega_{\rm rms}$, in comparison with $\langle V\rangle$ at $\alpha = 32$ deg. Minimum and incremental values of instantaneous ω are 1 and 0.75 s^{-1}, of $\langle\omega\rangle$ are 1 and 0.75 s^{-1}, and of $\omega_{\rm rms}$ are 0.5 and 0.5 s^{-1}. For contours of $\langle V\rangle$, units of numerical values designated on contour lines are mm/s and incremental value between contours is 2.5 mm/s.

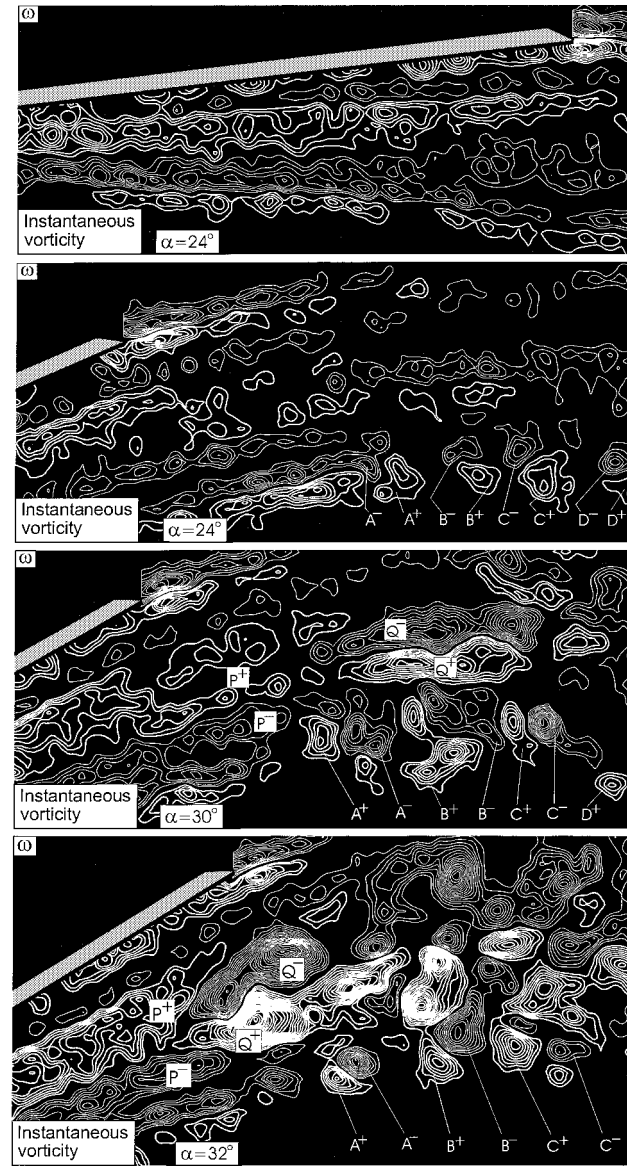

Fig. 3d Effect of angle of attack on patterns of instantaneous ω. Minimum and incremental values of ω for all cases are 1 and 0.75 s^{-1}.

the distance between the extrema of averaged positive and negative vorticity layers P^+ and P^- before the onset of vortex breakdown, as defined earlier. Over the range of 24 deg $\leq \alpha \leq$ 32 deg, representative values of λ for the small-scale, low-level concentrations are in the range $1.0 \approxeq \lambda/D_v \approxeq 1.6$. These values of dimensionless wavelength are smaller than those associated with the abrupt onset of vorticity concentrations in the vortex breakdown region, designated as Q^+ and Q^- in previous figures. A region of Q^+ contains, for example, a sequence of positive vorticity concentrations having a characteristic streamwise λ. Considering the range of angle of attack in Fig. 3d, the representative values of wavelength between Q^+ (or Q^-) concentrations of like sign lie in the range $1.7 \approxeq \lambda/D_v \approxeq 2.0$. Finally, the wavelength between the vorticity concentrations of like sign in the array A^+, A^- through D^+, D^- is also of interest. Over the range of angle of attack considered, this wavelength lies in the range $2.0 \approxeq \lambda/D_v \approxeq 3.0$. It should be emphasized that the same reference length scale D_v is used for all of these comparisons.

Consider the smallest-scale concentrations in the top image of Fig. 3d, also shown in Fig. 2. These concentrations are related to the layers P^+, P^-, R^+, R^- in the averaged image of Fig. 2. It is instructive to consider dimensionless length scales at a location where the concentrations in layers P and R are well developed. Choosing a distance $0.375C$ upstream of the trailing edge of the wing, the representative wavelength is $\lambda/D_v^* = 0.76$, in which D_v^* is the local diameter of the vortex. An alternate length scale for normalizing λ between these small-scale concentrations is $D_{\rm PR}$, defined as the distance across the vortex, measured from the interface between P^+ and R^- to the interface between P^- and R^+, as defined in the averaged image of Fig. 2. Values of $\lambda/D_{\rm PR}$ are approximately $\lambda/D_{\rm PR} = 0.48$, where $D_{\rm PR}$ is also evaluated at $0.375C$ upstream of the trailing edge of the wing. The physical basis for this normalization is that the small-scale concentrations of opposite sign in layers P^+ and R^- appear to form a counter-rotating system; likewise for the concentrations P^- and R^+. In fact, inspection of the locations of the peaks of the concentrations in layer R^+ in Fig. 2, for example, shows that they tend to occur at the valleys between the peaks of layer P^-. For the case of a free rotating vortex, the numerical simulation of Sreedhar and Ragab[5] shows generation of counter-rotating vortex pairs about the periphery of the vortex, apparently due to a centrifugal instability similar to the structures observed in a Taylor–Couette flow between rotating cylinders. Using the same definitions as in the foregoing, the wavelengths of these counter-rotating vorticity concentrations are in the range $0.46 \approxeq \lambda/D_{\rm PR} \approxeq 1.0$.

The Γ^* of the concentrations of azimuthal vorticity is defined as $\Gamma/\pi U_{\rm ref} D_v$, in which D_v is the prebreakdown diameter of the vortex and $U_{\rm ref}$ is a reference velocity; both of these parameters are defined in Sec. 2. It is evident from observing the instantaneous images in Fig. 3d that the largest values of circulation correspond to the concentrations of vorticity in the regions Q^+ and Q^-. At $\alpha = 30$ deg the

values of dimensionless circulation are in the range $0.4 \lessapprox \Gamma^* \lessapprox 0.5$, and at the high $\alpha = 32$ deg, they lie in the range $1.1 \lessapprox \Gamma^* \lessapprox 1.2$. These values compare with those of the individual concentrations of vorticity in the array A^+, A^- through D^+, D^-. For this array, the values of dimensionless circulation are in the range $0.1 \lessapprox \Gamma^* \lessapprox 0.4$ over the range of angle of attack considered. It is therefore evident that the higher values of circulation of the concentrations in the vortex array on the exterior of the vortex approach the lower values of those associated with vortex breakdown. Finally, the small-scale concentrations of vorticity in the vorticity layers below the wing, in absence of vortex breakdown (see top images of Figs. 2 and 3d), have values in the range $0.02 \lessapprox \Gamma^* \lessapprox 0.1$.

Qualitative Visualization of Flow Patterns

To gain further insight into the mechanism that gives rise to the instantaneous pattern of vorticity concentrations in the outer region of the vortex, described as concentrations A–D, dye visualization was undertaken. By changing the origin of the dye visualization marker, it was observed that vortices were shed from both the windward and leeward sides of the leading edge at an axial location near the trailing edge of the wing. Figure 4 shows dye visualization originating from a uniform layer of high density, which was spread along the windward side of the leading edge, and at a location near the trailing edge. The edge is defined by the sharp, angled, gray geometry in each of the visualization images. By using this type of dye visualization, as well as other locations of dye injection, it was observed that vortices are initially shed parallel to the leading edge of the wing, then undergo a rapid reorientation such that they are essentially vertical relative to the freestream. This process was characterized using a sequence of dye images taken with a high-resolution digital camera. Adjacent, nearly vertical concentrations of vorticity appear to form an inverted letter V, designated by the arrows in each dye image. It is suggested that the evolution of these concentrations of dye in Fig. 4 gives rise to the adjacent patterns of counter-rotating azimuthal vorticity A^+, A^-, and so on, indicated in Fig. 3d. It should be noted that rapid tilting of markers taken to represent shed vortices is evident in Fig. 6 of Riley and Lowson,[4] at locations farther upstream of the trailing edge, for a larger value of sweep angle, smaller angle of attack, and larger Reynolds number than the present values. Also evident in the dye visualization is a narrow band of lighter dye with its origin at the location designated by the arrow normal to the windward surface of the wing. Its trajectory is of the same form as that of small-scale longitudinal

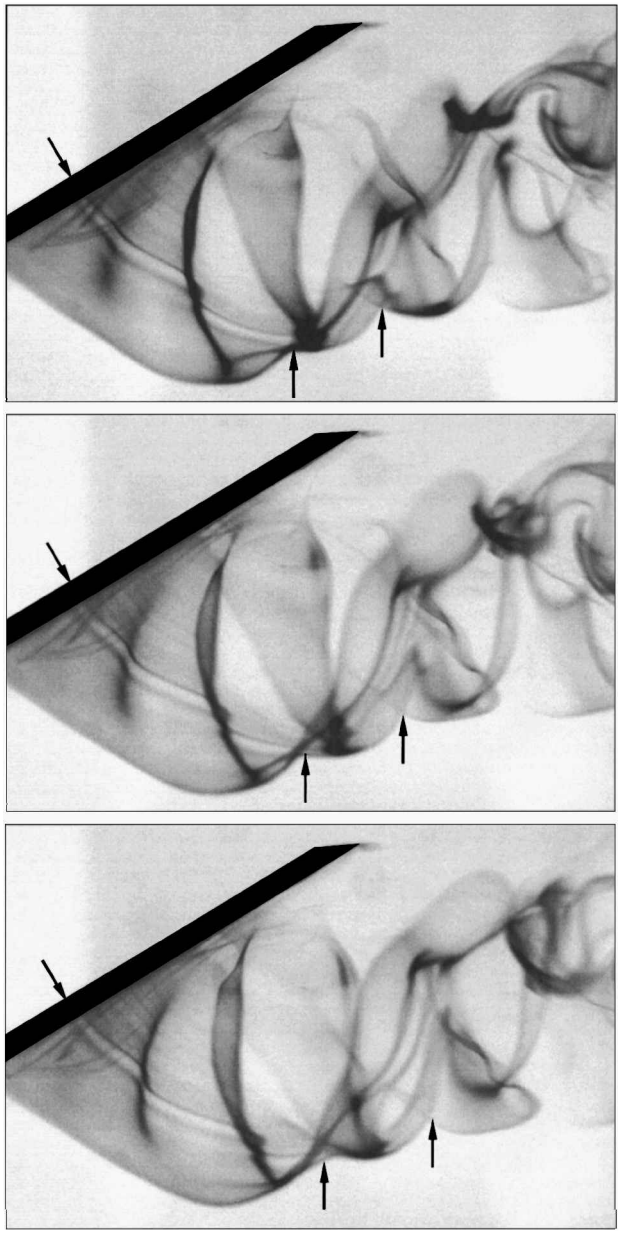

Fig. 4 Dye visualization of three-dimensional vortex shedding from the leading edge of the wing, at a chordwise location near the trailing edge; $\alpha = 32$ deg.

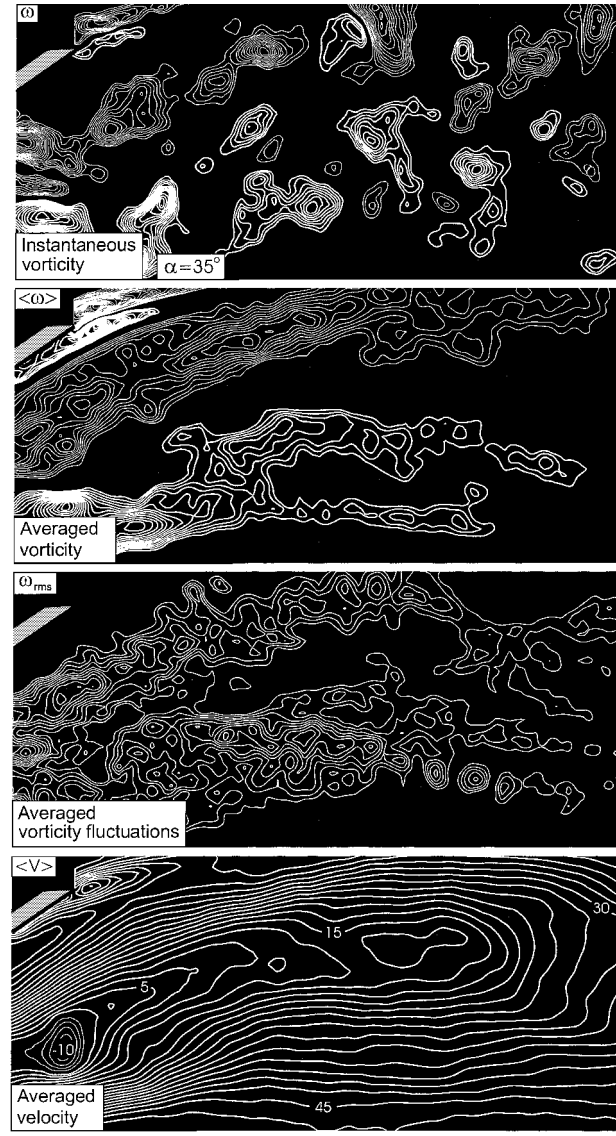

Fig. 5 Patterns of instantaneous ω, $\langle\omega\rangle$, and ω_{rms}, in comparison with $\langle V\rangle$ at $\alpha = 35$ deg. Minimum and incremental values of instantaneous ω are 2 and 0.75 s^{-1}, of $\langle\omega\rangle$ are 1 and 0.25 s^{-1}, and of ω_{rms} are 2 and 0.25 s^{-1}. For contours of $\langle V\rangle$, units of numerical values designated on contour lines are mm/s and incremental value between contours is 2.5 mm/s.

steady vortices visualized by Riley and Lowson.[4] This narrow band of lighter dye forms a knotlike structure with each of the vortices shed from the leading edge of the wing.

Downstream Evolution of Vorticity Concentrations

The issue arises as to the form of the broken-down leading-edge vortex at very high angle of attack and at locations downstream of the trailing edge of the wing. In particular, the associated wavelengths and circulation of the vorticity concentrations are of interest. The representative images of Fig. 5 correspond to $\alpha = 35$ deg. In this case, vortex breakdown occurs well upstream of the trailing edge of the wing, and the consequence for the instantaneous patterns of ω are indicated in the top image of Fig. 5. Large-scale clusters of positive and negative vorticity bound the wakelike region originating from the breakdown bubble. The representative streamwise wavelength of these vortical patterns is $\lambda/D_v^{**} \sim 2$, where the vortex diameter D_v^{**} is evaluated at the trailing edge of the delta wing, again by using the definition of distance between extrema of positive and negative as defined in Sec. 2. The circulation of these concentrations is relatively large, on the order of $\Gamma^* = 1.27$.

In accord with the trajectories of these large-scale clusters of vorticity, relatively high levels of ω_{rms} are generated along their paths. Moreover, the pattern of $\langle V \rangle$ indicates a wakelike structure; the centerline velocity of the wake increases with streamwise distance downstream of the breakdown bubble.

Criteria for Onset of Vortex Breakdown and Vorticity Fluctuations

Further insight into the onset of vortex breakdown for the conditions corresponding to Fig. 3c can be obtained by superposition of contours of constant $\langle \omega \rangle$ and constant $\langle V \rangle$, as shown in the top image of Fig. 6. This superposition of images zooms in on the region at the onset of vortex breakdown; it should be noted that intermediate contours of $\langle \omega \rangle$ and $\langle V \rangle$ have been omitted for purposes of clarity. Two crucial locations in the breakdown region are designated by a white dot and a black dot. The white dot represents the location of the switch in sign of azimuthal vorticity. Referring to Fig. 3c, it is the location where the abrupt transformation occurs between relatively distributed layers of positive and negative vorticity P^+ and P^- and highly concentrated regions of vorticity Q^+ and Q^-. In addition to the rapid onset of highly concentrated vorticity, the onset of vortex breakdown also involves a switch of the orientation of positive vorticity to a location relatively close to the wing surface. This switch is represented by concentration P^+ close to the wing surface and concentration Q^+ well away from the surface; the corresponding switch of the opposite sense occurs for P^- and Q^-. The black dot in the top image of Fig. 6 represents the apparent occurrence of a stagnation point along the centerline of the vortex. Upstream of this location, the mean (averaged) axial velocity is positive, and downstream of it, it takes on negative values. We therefore conclude that the switch in sign of azimuthal vorticity, represented by the white dot, precedes the occurrence of a stagnation point at the leading portion of the breakdown bubble. This observation is in accord with the theoretical model of Brown and Lopez.[13]

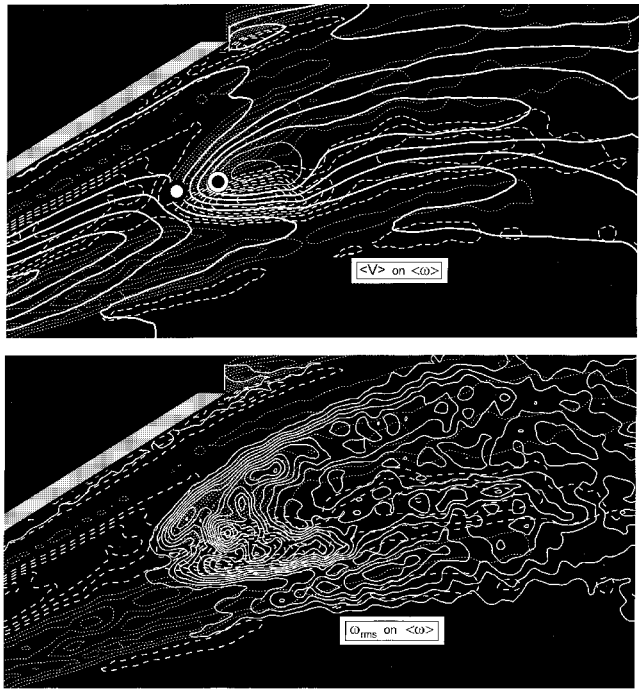

Fig. 6 Patterns of $\langle V \rangle$ on $\langle \omega \rangle$ and ω_{rms} on $\langle \omega \rangle$ at $\alpha = 32$ deg. Minimum and incremental values of $\langle \omega \rangle$ are 1 s^{-1} and 1.25 s^{-1} and for ω_{rms} values are 1 and 0.5 s^{-1}, respectively. For contours of $\langle V \rangle$, incremental value between contours is 10 mm/s. Negative and positive vorticity contours are represented by short and long dashed lines, respectively. Negative and positive velocity contours are designated by thin and thick solid lines, respectively.

Actually, the time-averaged structure of vortex breakdown shown in the top image of Fig. 6 is associated with substantial fluctuations of vorticity. Contours of constant ω_{rms} are superposed on contours of $\langle \omega \rangle$ in the image at the bottom of Fig. 6. A peak value of ω_{rms} occurs along the centerline of the vortex at a location coincident with the stagnation point. In fact, upstream of this location, on either side of the vortex centerline, two peak values of ω_{rms} occur. Taken together, these three peak values of ω_{rms} show that the onset of vortex breakdown is associated with large values of local vorticity fluctuations. The largest peak value of ω_{rms} is 7.92 s^{-1}; it compares with the peak value of $\langle \omega \rangle = 10.8$ s^{-1}. A further observation is that significant levels of ω_{rms} occur at approximately the location of the switch in sign of $\langle \omega \rangle$, designated by the large white dot in the top image of Fig 6.

Conclusions

Using an approach of global, instantaneous imaging of the leading-edge vortex from a delta wing, it has been demonstrated that multiple layers of instantaneous and averaged azimuthal vorticity can coexist over a range of angle of attack. From the standpoint of buffet-induced loading of aerodynamic surfaces, the instantaneous structure of these vorticity layers, and the variation of this structure with time, are of principal importance. Three basic classes of vorticity concentrations are evident. They are classified according to their physical origin in Table 1, and briefly summarized in the following:

1) Concentrations of azimuthal vorticity due to a centrifugal instability of the vortex have relatively small values of wavelength and circulation. The wavelength normalized by the local vortex diameter is in general accord with the recent numerical simulation of Sreedhar and Ragab[5] for a free vortex in absence of a leading edge.

2) Concentrations due to vortex breakdown have significantly larger values of wavelength and large values of circulation. They are associated with the classical helical mode instability of breakdown.

3) Concentrations due to an unsteady instability from the leading edge have relatively large values of wavelength and moderate values of circulation. They apparently arise from reorientation of the unsteady layer vorticity shed from the leading edge. In concept, their origin appears to be the same as shown by smoke visualization of the time-varying instability of Riley and Lowson.[4]

It should be emphasized that the wavelength and circulation of certain of these classes of vorticity concentrations may be a function of Reynolds number. For example, the third class is expected to scale on the thickness of the shear layer shed from the leading edge. This aspect deserves further consideration for all classes of concentrations. It is well known, however, that the onset of breakdown of a vortex from a sharp leading edge is relatively insensitive

Table 1 Dimensionless wavelength and circulation of classes of azimuthal vorticity concentrations

Parameter	λ/D_v	$\Gamma^* = \Gamma/\pi U_{\text{ref}} D_v$
Concentrations arising from centrifugal instability	$1.0 \lessapprox \lambda/D_v \lessapprox 1.6$	$0.02 \lessapprox \Gamma^* \lessapprox 0.1$
Concentrations due to vortex breakdown	$1.7 \lessapprox \lambda/D_v \lessapprox 2.0$	$0.4 \lessapprox \Gamma^* \lessapprox 1.2$
Concentrations due to instability from the leading edge	$2.0 \lessapprox \lambda/D_v \lessapprox 3.0$	$0.1 \lessapprox \Gamma^* \lessapprox 0.4$

to Reynolds number. This observation should be correlated with the wavelength and scale of the first and third classes of concentrations. The possible Reynolds number dependence may influence the relative importance of the classes of vorticity concentration for buffeting of the surface of a wing or tail. Present characterizations suggest that the first class may not be important, in view of their relatively small wavelength and circulation. In future investigations, these considerations could be incorporated with images of the flow structure in crossflow planes, in addition to the plane employed in this study.

A major emphasis of this investigation has been on the instantaneous and averaged structure of the leading-edge vortex before, and in the vicinity of, the onset of vortex breakdown. An important, related aspect is the identification and comparison of two different criteria for the onset of vortex breakdown and their interpretation in relation to vorticity fluctuations. The first criterion involves the location of the switch of azimuthal vorticity, and the second involves occurrence of a stagnation point along the centerline of the vortex. It is shown that the former criterion precedes the latter, and this sequence of events is consistent with the concept of Brown and Lopez,[13] who established the relationship between the change in sign of the azimuthal vorticity and the occurrence of zero axial velocity along the centerline of the vortex. Particularly interesting, however, is the occurrence of peak levels of vorticity fluctuation (i.e., rms vorticity) in relation to these criteria for onset of vortex breakdown. At the location of the stagnation point, a large peak of ω_{rms} occurs. Moreover, two additional peaks occur upstream of this location, immediately following the switch in sign of the averaged azimuthal vorticity. In other words, the onset of the switch of the mean vorticity also marks the occurrence of significant levels of vorticity fluctuation. In fact, the peak values of ω_{rms} at the onset of vortex breakdown are of the same order as the peak values of $\langle\omega\rangle$.

Acknowledgments

The authors gratefully acknowledge the financial support of the Air Force Office of Scientific Research under Contract F49620-99-1-0011, monitored by Steven Walker. One of the authors, Besir Sahin, would like to thank the Scientific and Technical Research Council of Turkey (TUBITAK) and NATO for their financial support.

References

[1]Gursul, I., and Xie, W., "Buffeting Flows Over Delta Wings," *AIAA Journal*, Vol. 37, No. 1, 1999, pp. 58–65.

[2]Earnshaw, P. B., and Lawford, J. A., "Low Speed Wind Tunnel Experiments on a Series of Sharp-Edged Delta Wings," Aeronautical Research Council, R& M 3424, London, Aug. 1964.

[3]Mabey, D. B., "Beyond the Buffet Boundary," *Aeronautical Journal*, Vol. 77, April 1973, pp. 201–215.

[4]Riley, A. J., and Lowson, M. V., "Development of a Three-Dimensional Free Shear Layer," *Journal of Fluid Mechanics*, Vol. 369, 1998, pp. 49–89.

[5]Sreedhar, M., and Ragab, S., "Large Eddy Simulation of Longitudinal Stationary Vortices," *Physics of Fluids*, Vol. 6, No. 7, 1994, pp. 2501–2514.

[6]Sarpkaya, T., "On Stationary and Travelling Vortex Breakdowns," *Journal of Fluid Mechanics*, Vol. 45, Pt. 3, 1971, pp. 545–559.

[7]Sarpkaya, T., "Vortex Breakdown in Swirling Conical Flows," *AIAA Journal*, Vol. 9, No. 9, 1971, pp. 1792–1799.

[8]Sarpkaya, T., "Effect of the Adverse Pressure Gradient on Vortex Breakdown," *AIAA Journal*, Vol. 12, No. 5, 1974, p. 607.

[9]Hall, M. G., "Vortex Breakdown," *Annual Review of Fluid Mechanics*, Vol. 4, 1972, pp. 195–218.

[10]Liebovich, S., "Structure of Vortex Breakdown," *Annual Review of Fluid Mechanics*, Vol. 10, 1978, pp. 221–246.

[11]Liebovich, S., "Vortex Stability and Breakdown: Survey and Extension," *AIAA Journal*, Vol. 22, No. 9, 1984, pp. 1192–1206.

[12]Escudier, M., "Vortex Breakdown: Observations and Explanations," *Progress in Aerospace Sciences*, Vol. 25, No. 2, 1988, pp. 189–229.

[13]Brown, G. L., and Lopez, J. M., "Axisymmetric Vortex Breakdown. Part 2. Physical Mechanisms," *Journal of Fluid Mechanics*, Vol. 221, No. 1, 1990, pp. 553–576.

[14]Lopez, J. M., and Perry, A. D., "Axisymmetric Vortex Breakdown. Part 3. Onset of Periodic Flow and Chaotic Advection," *Journal of Fluid Mechanics*, Vol. 234, No. 1, 1992, pp. 449–471.

[15]Delery, J. M., "Aspects of Vortex Breakdown," *Progress in Aerospace Sciences*, Vol. 30, No. 1, 1994, pp. 1–59.

[16]Visbal, M. R., "Onset of Vortex Breakdown Above a Pitching Delta Wing," *AIAA Journal*, Vol. 32, No. 8, 1994, pp. 1568–1575.

[17]Rusak, Z., Wang, S., and Whiting, C. H., "The Evolution of a Perturbed Vortex in a Pipe to Axisymmetric Vortex Breakdown," *Journal of Fluid Mechanics*, Vol. 366, No. 1, 1998, pp. 211–237.

[18]Wérle, H., "Sur l'Éclatement des tourbillons," Note Technique No. 175, ONERA, 1971.

[19]Pagan, D., and Solignac, J. L., "Experimental Study of the Breakdown of a Vortex Generated by a Delta Wing," *Recherche Aérospatiale*, Vol. 3, 1986, pp. 29–51.

[20]Towfighi, J., and Rockwell, D., "Instantaneous Structure of Vortex Breakdown on a Delta Wing via Particle Image Velocimetry," *AIAA Journal*, Vol. 31, No. 6, 1993, pp. 1160–1162.

[21]Lin, J.-C., and Rockwell, D., "Transient Structure of Vortex Breakdown on a Delta Wing at High Angle of Attack," *AIAA Journal*, Vol. 33, No. 1, 1995, pp. 6–12.

[22]Visbal, M. R., "Structure of Vortex Breakdown on a Pitching Delta Wing," AIAA Paper 93-0434, January 1993.

[23]Gad-el-Hak, M., and Blackwelder, R. F., "The Discrete Vortices from a Delta Wing," *AIAA Journal*, Vol. 23, No. 3, 1985, pp. 961, 962.

[24]Gad-el-Hak, M., and Blackwelder, R. F., "Control of the Discrete Vortices from a Delta Wing," *AIAA Journal*, Vol. 26, No. 5, 1986, pp. 1042–1049.

[25]Lowson, M. V., "The Three Dimensional Vortex Sheet Structure on Delta Wings," *Fluid Dynamics of Three-Dimensional Turbulent Shear Flows and Transition*, CP-438, AGARD, 1988.

[26]Gordnier, R. E., and Visbal, M. R., "Instabilities in the Shear Layer of Delta Wings," AIAA Paper 95-2281, June 1995.

[27]Visbal, M. R., and Gordnier, R. E., "Origin of Computed Unsteadiness in the Shear Layer of Delta Wings," *Journal of Aircraft*, Vol. 32, No. 5, 1995, pp. 1146–1148.

[28]Cipolla, K., and Rockwell, D., "Small-Scale Vortical Structures in Crossflow Plane of a Rolling Delta Wing," *AIAA Journal*, Vol. 36, No. 12, 1998, pp. 2276–2278.

[29]Payne, F. M., "The Structure of Leading Edge Vortex Flows Including Vortex Breakdown," Ph.D. Dissertation, Dept. of Aerospace and Mechanical Engineering, Univ. of Notre Dame, Notre Dame, IN, 1987.

[30]Payne, F. M., Ng, T. T., Nelson, R. C., and Schiff, L. B., "Visualization and Wake Surveys of Vortical Flow Over a Delta Wing," *AIAA Journal*, Vol. 26, No. 2, 1988, pp. 137–143.

[31]Reynolds, G. A., and Abtahi, A. A., "Three-Dimensional Vortex Development, Breakdown, and Control," AIAA Paper 89-0998, March 1989.

[32]Su, W., Liu, M., and Lui, Z., "Topological Structures of Separated Flows About a Series of Sharp-Edged Delta Wings at Angles of Attack up to 90°," *Topological Fluid Mechanics, Proceedings of the IUTAM Symposium*, edited by H. K. Moffatt and A. Tsinber, Cambridge Univ. Press, Cambridge, England, U.K., 1990, pp. 395–400.

[33]Rockwell, D., Magness, C., Towfighi, J., Akin, O., and Corcoran, T., "High-Image-Density Particle Image Velocimetry Using Laser Scanning Techniques," *Experiments in Fluids*, Vol. 14, No. 3, 1993, pp. 181–192.

J. C. Hermanson
Associate Editor